DEFENCE RESEARCH ESTABLISHMENT
PACIFIC
VICTORIA, B.C.

Reprint 74-8

# WIND NOISE UNDER WINTER ICE FIELDS

by
A.R. Milne

DEFENCE RESEARCH BOARD
CANADA

# Wind Noise Under Winter Ice Fields

A. R. MILNE

*Defence Research Establishment Pacific, Victoria, British Columbia, Canada*

Wind blowing over a snow layer on sea ice produces noise in the water beneath as a result of a multitude of snow grain impacts on the upper boundary of the snow. These impacts are caused by the downwind flow of saltating snow grains, which extract energy from the wind. Saltation of snow grains and the noise commence at a threshold wind speed sufficient to dislodge loose snow grains at the snow-air boundary. The resulting spectrum of the noise in the 400-Hz to 20-kHz band, sensed by a hydrophone in the water below, depends on the acoustic impulse responses of the paths between the snow grain impacts and the hydrophone. As a consequence, above the threshold wind speed the shape of the underice noise spectrum at a given site will remain constant, subject to changes in the snow and ice layers; however, the noise intensity will increase with the wind speed. The application of Bagnold's (1941) theory of blown sand shows that the noise intensity increases as the cube of the wind speed above the threshold speed for saltation. Comparisons with experimental measurements of wind noise intensity versus wind speed support this dependence. The noise intensity is independent of snow grain size and depends primarily on the snow grain flow.

A layer of ice on the sea not only inhibits the formation of wind waves and swell but in the winter and springtime forms a solid support for snow to drift upon and migrate across when the wind blows. The wind blowing over sea ice produces noise in the water beneath, which has been described by *Ganton and Milne* [1965] and *Milne et al.* [1967]. However, there has been no satisfactory explanation of the actual mechanism of noise production. Ganton and Milne postulated that wind noise is generated by vortex shedding of turbulent eddies produced when the amplitude of the surface roughness exceeds the thickness of the laminar sublayer. Although it is possible that this mechanism does in part contribute to the noise detected by a hydrophone under the sea ice, a more satisfactory explanation based on direct observations of cause and effect is as follows: When the wind speed exceeds a small threshold value, grains of snow are dislodged from the boundary. These grains extract energy from the wind and gain speed; then they fall to the boundary downwind, whereupon more grains are dislodged by the impacts. The impacts on the boundary produce noise that is transmitted through the layers of snow and sea ice into the water beneath. This saltating activity has been described by *Bagnold* [1941, pp. 16–20] in application to windblown sand and by *Oura et al.* [1967] for snow particles.

It is important to distinguish snow in the form of falling flakes from particles of snow that have been mechanically abraded under wind action and are transported near and at the surface. The particles of snow range from dust-size motes that remain airborne in a turbulent wind to millimeter-size grains of snow that remain near the surface when they are driven by the wind. It is these grains of snow that appear to be important in the generation of wind noise in the water.

Recently, underice wind noise spectra were obtained during March and April 1972 from camps located in Lancaster Sound, south of Devon Island, and in Robeson Channel (Figure 1). Although these observations were made at sites within the Canadian arctic archipelago, it is likely that similar spectra would be observed for winds blowing over sea ice of a similar nature in other polar regions. In Lancaster Sound the sea ice had a relatively uniform thickness of 183 cm, upon which was an irregular snow layer averaging 10 cm in thickness. The camp in Robeson Channel was centrally situated on a large, smooth, frozen lead of 137-cm-thick winter ice that had a relatively uniform 4.0-cm thickness of snow adhering to it. In this location the main instrumental sensors (Figure 2) were a broad band hydrophone at a depth of 30 m, a microphone situated at the upper surface of the ice, a microphone situated at the upper surface of the snow, and an anemometer arranged with a vertical traversing mechanism for obtaining wind speed profiles. The three acoustic sensors could be connected in sequence to a real-time spectrum analyzer so that noise spectra could be obtained quickly in response to changes in wind speed. Visual observations of drifting snow grains and audio monitoring of the underwater noise aided in the phenomenological interpretation. Silent operation of the camp during the recording of real-time spectra was achieved by using electrical power from storage batteries. Periods of recording were chosen to minimize contamination of the spectra by impulses of sound from cracking ice. Contamination of this form was easily recognized but occurred infrequently because of the viscous nature of the winter ice in both camp areas [*Milne*, 1972]. Unfortunately, a desirable selection of wind speeds did not occur this year in either of the two camp locations, so that variations of noise intensity with wind speed from previous experiments are used in the support of theoretical results.



## OBSERVED NOISE SPECTRA

All spectra were recorded on a plotter connected to the output of a real-time spectrum analyzer (Spectral Dynamics type SD302A). Each spectrum consisted of a 64-ensemble average, the analyzer set on the 20-kHz upper frequency limit, with an ensemble sweep time of 0.05 s. The lower frequency limit for each spectrum was set by the use of a 400-Hz high-pass filter at the input to the analyzer. High-pass filtering was necessary to eliminate high-amplitude low-frequency fluctuations in noise, which could not be accommodated by the dynamic range of the analyzer, and at the same time to accommodate the higher-frequency range of interest.

Figure 3 shows three spectra for wind-induced underwater noise sensed by the hydrophone at 30-m depth at the Robeson Channel site. Figures 4 and 5 show wind-induced noise spec-

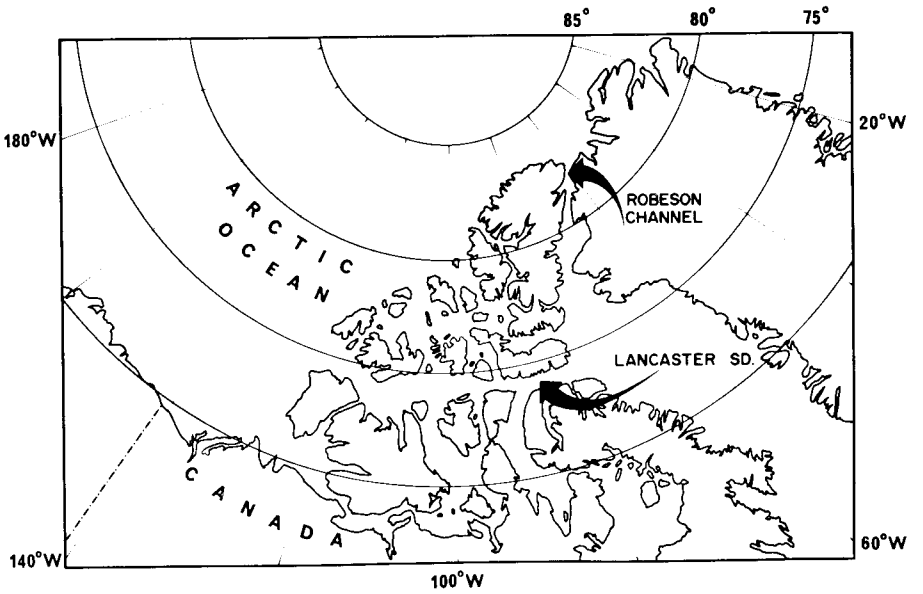


Fig. 1. Locations of experimental sites in Robeson Channel and Lancaster Sound during April 1972.

tra from microphones at the snow-ice boundary and the air-snow boundary, respectively, also at the Robeson Channel site. Figure 6 shows spectra of underwater noise sensed by a hydrophone at 30-m depth in Lancaster Sound for two different mean wind speeds.

To obtain some idea of the relative spectral response of a hydrophone in the water, compared with that of a microphone at the snow-ice boundary, to noises other than those from snow grain saltations, spectra were recorded for 'snow-crunching' noises from a man's footsteps. The snow-crunching noises were generated by a man continuously walking in short rapid steps in the snow in a circle of 6-m radius centered on the hydrophone hole and microphone cavity. Figure 7 shows the snow-crunching noise spectrum from the hydrophone at 30-m depth, and Figure 8 shows the completely different spectra from the microphone for the same noises.

These results and disparities between wind-induced noise spectra sensed by a hydrophone in the water and those sensed by microphones at the snow boundaries can be explained as effects created by propagation of sound across and within the snow and ice layers.

## Relationship of Snow Grain Movement to Noise

Observations of snow grain movement and continuous displays of real-time spectra at 3.2-s intervals soon established the coincidence of the onset of snow grain movement with a rise in the underwater noise level from levels previously close to those of hydrophone system noise. At wind speeds near the threshold for grain dislodgement, wind gusting was clearly related to temporary and abrupt increases in the underwater noise level, with accompanying sounds similar to those made by a handful of sand thrown on a metal roof. Later, as the mean wind speed at 3-m height increased, the time intervals when spectra collapsed to system noise levels shortened and then disappeared; the spectra then became remarkably stable, with shapes independent of the wind speed. This stability appeared to conform to the visual uniformity of the drift rate of the snow grains as they flowed in sinuous paths over the snow on the sea ice, despite the fact that gusting of the wind was a normal state at an anemometer height of 3 m. *Bagnold*'s [1941, p. 57] explanation of how sand movement profoundly

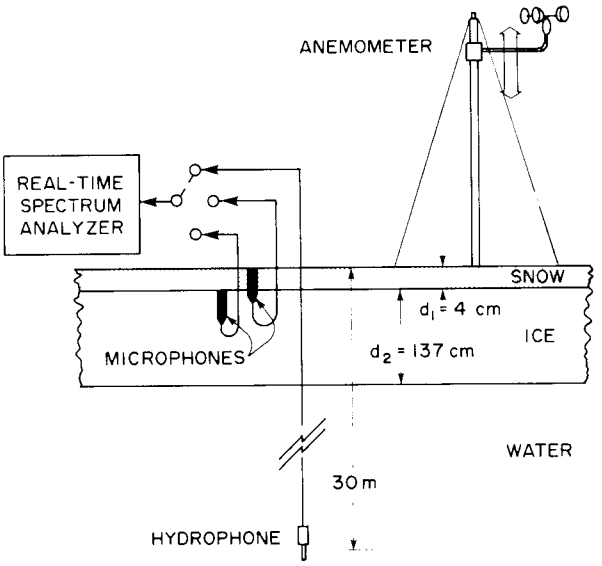


Fig. 2. Sensor system at the Robeson Channel site.

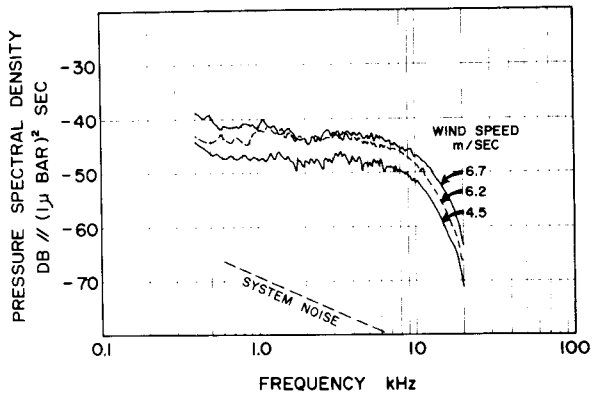


Fig. 3. Spectra for wind-induced underwater noise sensed by an omnidirectional hydrophone at a depth of 30 m in Robeson Channel. The snow layer had a mean thickness of 4 cm, and the sea ice was 137 cm thick.

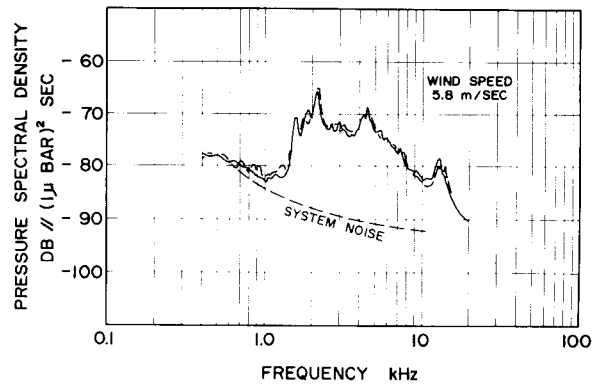


Fig. 4. Spectra for wind-induced noise sensed by a microphone at the snow-ice boundary in Robeson Channel.

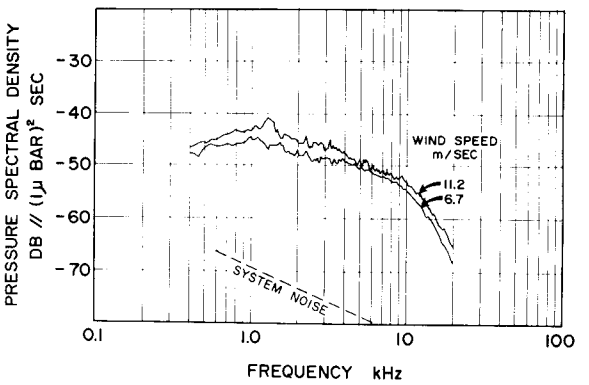


Fig. 6. Spectra for wind-induced underwater noise sensed by an omnidirectional hydrophone at a depth of 30 m in Lancaster Sound. The snow layer had a mean thickness of 10 cm, and the sea ice was 0.03 cm thick.

alters the state of the surface wind supports these observations. He observed that once grain movement, or saltation, has commenced, the wind speed in the grain-laden surface layer becomes almost independent of the wind speed above the layer, no matter how hard it blows. Stronger winds tend to thicken the grain-laden surface layer. In terms of noise production from saltating snow grains this means that a higher average surface impact rate occurs and results in a corresponding uniform increase in underwater noise with increased wind speeds.

Many of Bagnold's results are directly applicable to the physics of drifting snow. For example, the fluid threshold wind speed at a height of 3 m for grain movement to commence can be calculated for assumed neutral air conditions if the grain size is known. Bagnold showed that the fluid threshold wind speed $v_t(z)$ at a height $z$ is given by

$$v_t(z) = 0.575\ [ga_1(\sigma - \rho_0)/\rho_0]^{1/2}\ \log_{10}\ (z/z_1)$$

where $g$ is the acceleration due to gravity, $a_1$ is the minimum grain diameter, $\sigma$ is the grain density, $\rho_0$ is the density of air, and $z_1$ is the aerodynamic roughness (here $z_1$ is equated to 1/30 of the mean grain diameter). In Robeson Channel, measured grain sizes ranged between 0.025- and 0.075-cm diameter for those grains loosely accumulated in shallow surface depressions, most grains being near 0.075 cm in diameter. Therefore, by using values of $z_1 = (0.075/30)$ cm, $z = 300$ cm, $a_1 = 0.025$ cm, $g = 981$ cm/sec$^2$, $\sigma = 0.99$ g/cm$^3$, and $\rho_0 = 1.22 \times 10^{-3}$ g/cm$^3$, the threshold wind speed $v_t(z)$ at an anemometer height of 3 m is calculated as 4.1 m/sec. This value corresponds closely to observed wind speeds for the threshold of grain movement entered into the field log, which ranged between 3.6 and 4.0 m/sec. It is interesting to note that once $v_t(z)$ is exceeded for small-size grains, impacts with larger grains can sustain grain saltation for a wide range of grain sizes.

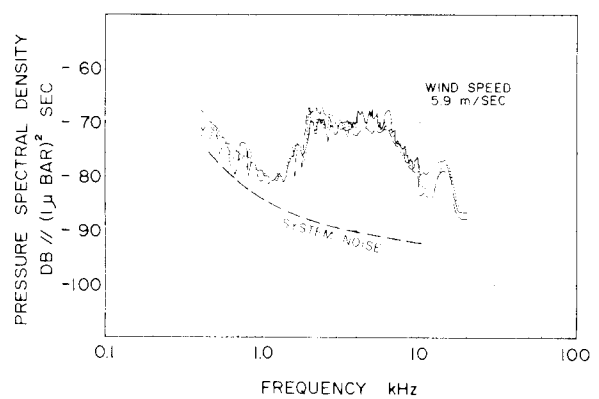


Fig. 5. Spectra for wind-induced noise sensed by a microphone at the air-snow boundary in Robeson Channel.

Of more importance to the generation of underwater noise is the relationship of the flow of snow grains with the wind speed. *Bagnold* [1941, p. 69] showed that the sand flow $q$, which is the mass of sand grains flowing per second past a given point in a lane of unit width, is proportional to the cube of an excess wind speed as follows:

$$q \propto a_2^{1/2}[v(z) - V_t]^3 \quad \text{g/sec}^{-1}\ \text{cm}^{-1}$$

for $v(z) > v_t(z)$ only. Here $a_2$ is the mean grain diameter, and $V_t$ is a constant equal to the threshold wind speed at a particular height $z$. Figure 9 illustrates the heights $z$, $z_1$, and $z_0$ and the wind speeds $v(z)$, $v_t(z)$, and $V_t$. Theoretically, the intersection of the threshold wind speed profile (dashed line) and families of profiles for higher wind speeds (one is shown by a solid line) occurs at the constant threshold wind speed $V_t$ at height $z_0$. Therefore, when snow grains commence moving under neutral air conditions, the aerodynamic roughness $z_1$ (measured as the intersection on the $z$ axis of the wind speed profile) will rise abruptly and become dependent on the wind speed. Experimentally, this change in $z_1$ has been measured by *Oura et al.* [1967] from wind speed profiles obtained over snow fields and during blowing snow.

The solid line in Figure 9 is a least squares fit to wind speed measurements made in Robeson Channel, where the average wind speed $v(z)$ at $z = 3$ m was 9.3 m/sec under conditions of blowing snow, whereas the dashed line is a calculated threshold profile obtained by using the values of $v_t(300)$ and $z_1$ calculated earlier. The measured profile with points indicated by small squares shows averages obtained during 10 vertical traverses of the anemometer over a 90-min interval. At each height in a given traverse, counts of anemometer revolutions were made for 60 s, all counts for all traverses being averaged for the 90-min interval during which average wind speeds and direction remained reasonably constant. The straight line implies that the mean wind varied logarithmically with height according to neutral conditions of atmospheric stability, where

$$v(z) = (V_*/\kappa)\ \ln\ (z/z_1) = 5.75\ V_*\ \log_{10}\ (z/z_1) \quad \text{cm sec}^{-1}$$

where $V_*$ is the drag velocity, $\kappa$ is the von Karman constant, set equal to 0.40, and $z_1$ is the aerodynamic roughness.

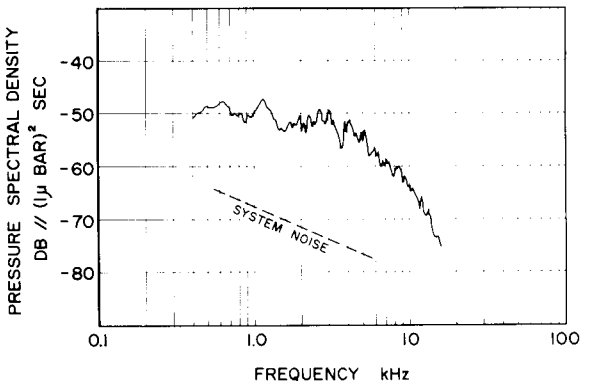


Fig. 7. A spectrum of underwater noise resulting from the crunching noise of footsteps on the snow. An omidirectional hydrophone was at a depth of 30 m in Robeson Channel.

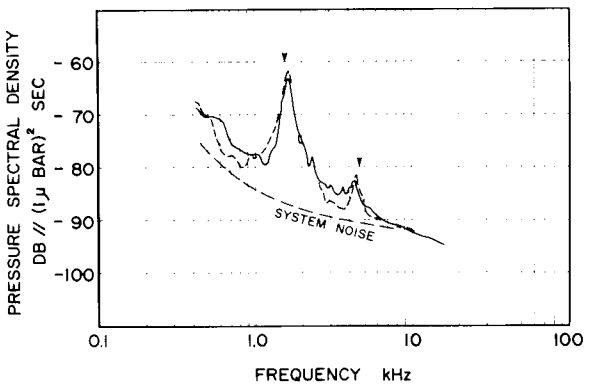


Fig. 8. Spectra of noise detected by a microphone at the snow-ice boundary resulting from the crunching noise of footsteps on the snow at the Robeson Channel site. Spectral peaks (arrows) are identified as the first and second modes for Crary waves in sea ice of 137-cm thickness.

*Bagnold* [1941, p. 64] also showed that the flow $q$ is directly proportional to the total impact momentum loss rate per unit area of the surface for the saltating grains. As a result, the formula for $q$ also predicts the change in the noise power produced per unit of surface area, which will rise abruptly as the wind speed increases to $v_t(z)$ and will continue to rise at a rate approaching the cube of the wind speed for high wind speeds. Practically, the effect of wind gusting and the integration of wind noise over a large area by the hydrophone eliminates any abrupt rise in the observed noise power with increasing mean wind speeds.

Figure 10 (top) shows measured wind noise levels in the 3.2- to 6.4-kHz band versus wind speed at an anemometer height of 5 m from *Ganton and Milne* [1965] and *Milne et al.* [1967]. (The anomalous data points, marked by open circles [*Milne et al.*, 1967], represent noise observations that were obtained during a period of heavy snow precipitation and increasing air temperatures, while the wind speed was relatively constant. The noise progressively decreased during this nontypical period.) These wind noise levels are to be compared with the curves in the bottom of Figure 10, which shows a family of calculated curves from the formula for the snow grain flow $q$ versus the wind speed for $z = 3$ m. The family parameter is the mean grain size $a_2$ in centimeters. The threshold wind speeds $V_t$ and $v_t(z)$ are proportional to $a_1^{1/2}$, where $a_1$ is the minimum grain size set equal to $a_2/3$. Except for threshold wind speeds these curves show that the snow grain flow, and therefore the impact momentum loss rate, is virtually independent of the mean grain size. The apparent independence of the snow grain flow with respect to grain size is supported by *Dyunin*'s [1967] theoretical development of the snow-transporting ability of the wind.

From Figure 10 and the previous discussion it can be concluded that, at different times and locations, differences in underice wind noise spectra will occur mostly as a result of differences in the transmission paths of sounds from grain impacts through the snow and ice layers to the water beneath. Another conclusion is that the noise intensity caused by the wind would be expected to rise in proportion to the cube of the wind speed for high wind speeds, which is equivalent to a 9-dB increase in intensity for a doubling of the wind speed.

## Noise Spectra Related to Snow and Ice Layers

The snow layer on sea ice in cold weather is a somewhat rigid foamlike material formed of snow granules adhering to each other. This layer also has variable mechanical properties and is firmly bonded to the sea ice. Its exposed upper surface often has raised patches that are glazed and smooth; the slight depressions surrounding these patches act as catch basins for mobile snow grains. Consequently, saltating snow grains, which strike the snow surface at small acute angles, will bounce from glazed patches or transfer momentum to loose grains in the depressions. Impulsive forces resulting from snow grain impacts can be resolved in both vertical downward and horizontal downwind directions at the rough upper boundary of the snow layer. The net horizontal component of the impulsive forces tends to move the ice sheet downwind, while the fluctuating component provides excitation for horizontal shear, or *SH*, waves. The vertical component of the impulsive forces can excite longitudinal, or *P*, waves as well as vertically polarized shear, or *SV*, waves. These various waves in layered media are described by *Ewing et al.* [1957]. Those *SH* waves that propagate in the ice layer cannot leak into the water and are therefore unimportant as contributors to underice noise. In general then the vertical im-

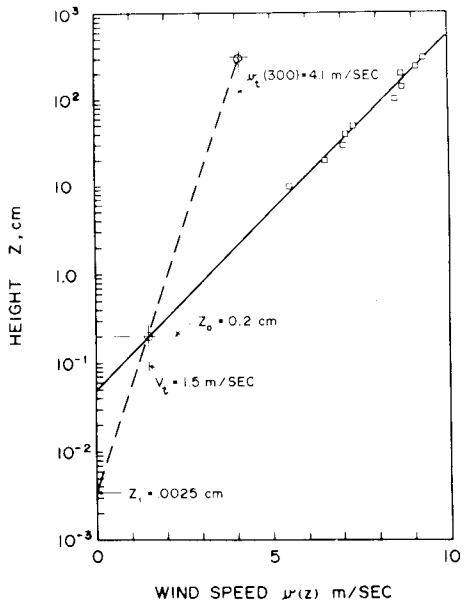


Fig. 9. An averaged wind speed profile from the Robeson Channel site. The solid line is a least squares fit to the points shown as squares, and $v_t$ (300) is the threshold wind speed at a height of 300 cm for the onset of snow grain movement.

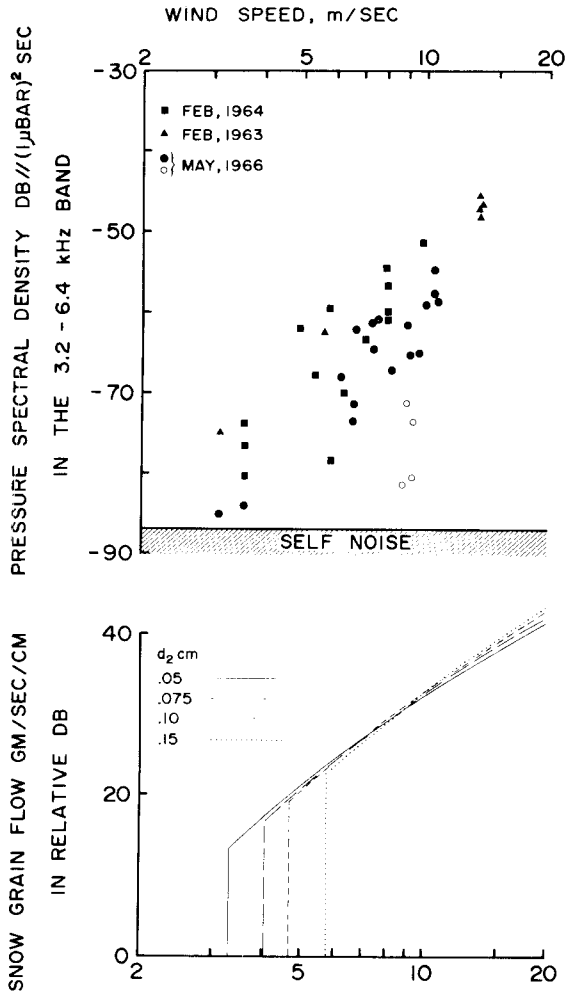


Fig. 10. (Top) Experimental wind noise levels in the 3.2- to 6.4-kHz frequency band versus wind speed at an anemometer height of 5 m. (Bottom) Calculated snow grain flow versus wind speed for $z = 3$ m, $d_2$ being the mean grain diameter in centimeters.

pact forces, which excite $P$ waves and $SV$ waves, are of importance. The $P$ waves would be expected to predominate over other wave types when impacts occur in loose grains. Only a small fraction of the amplitude of $SV$ waves in the ice layer will convert to $P$ waves in the water, and only if the phase velocity for waves in the ice layer exceeds the speed of sound in water. An exception to this latter condition exists for Crary waves, which are special $SV$ waves, where the phase velocity in the ice layer is close to the speed for longitudinal waves in the ice. These waves can propagate without leakage of $P$ waves to the water, and their modes have almost constant frequencies.

As a consequence, the hydrophone in the water beneath the ice responded to a uniform surface distribution of impulsive sounds from saltation impacts that were transmitted downward through the snow and ice layers, whereas the microphones responded to waves propagating within the layers and to localized surface noise. This difference in response is clearly evident where snow-crunching noises from footsteps on the snow produced the underwater noise spectrum of Figure 7 and at the same time produced the very different spectrum at the ice-snow boundary shown in Figure 8. The two spectral peaks in Figure 8 correspond to the first two modes of Crary waves. For this type of $SV$ wave the frequencies corresponding to mode number $n$ are given by

$$f = (2n + 1)(1/\beta_2^2 - 1/\alpha_2^2)^{-1/2}/d_2 \quad \text{Hz}$$

where $d_2$ is the ice thickness in meters, $\alpha_2$ is the speed for compressional body waves in the ice in meters per second, and $\beta_2$ is the speed for shear body waves in the ice in meters per second. For $d_2 = 1.37$ m, $\alpha_2 = 3380$ m/sec, and $\beta_2 = 1825$ m/sec, calculations show that first-mode frequency is 1583 Hz and the second-mode frequency is 4748 Hz. These two frequencies are marked by small arrows in Figure 8. Footsteps appear to excite $SV$ and $P$ waves strongly, all of which leak most of their energy into the water with the exception of the Crary wave, which is trapped. The microphone was sensitive to $P$ waves only, so that a small fraction of the Crary wave energy must have been converted to $P$ waves at the discontinuity provided by the cylindrical cavity within which the microphone was situated.

The spectra in Figure 4, from the microphone located at the snow-ice boundary, exhibit an abrupt rise for increasing frequencies at 1.4 kHz from levels close to system noise. This rise in intensity most likely corresponded to the onset of the first $P$ wave mode in the ice layer. For example, if it is assumed that the ice layer is a free plate, the cutoff frequency for the first $P$ wave mode is given by $f_c = \alpha_2/(2d_2)$ Hz [*Brekhovskikh*, 1960, p. 73]. For $\alpha_2 = 3380$ m/sec and $d_2 = 1.37$ m, $f_c = 1.23$ kHz. The spectra from the microphone at the air-snow boundary (Figure 5) show somewhat similar characteristics. Interpretation of other spectral features in Figures 4 and 5 is not warranted because of the uncertainties in the coupling of various plate waves to the cylindrical cavities within which the microphones were mounted; however, it is likely that both microphones responded almost solely to plate waves propagating within the ice and not to sounds propagating within the highly attenuating snow layer.

Snow grain saltation noise produced spectral responses in omnidirectional hydrophones in the water beneath the ice such as those shown in Figures 3 and 6. These responses depended on a number of factors that vary with acoustic frequency. The main factors are the spectral response of the snow grain impact energy loss, the scattering loss within and at the boundaries of the snow and ice layers, and the reflection and transmission coefficients at their boundaries. The attenuation, reflection, and transmission coefficients are the only ones of these for which either experimental data are available or values can be readily calculated for modeling purposes.

## CALCULATED HYDROPHONE WIND NOISE SPECTRA

Figure 11 shows calculated underwater acoustic noise pressure spectra for ice and snow thicknesses corresponding to those measured at the Robeson Channel and Lancaster Sound sites. The lower-intensity curve, applicable to the Lancaster Sound site, results from a thicker snow cover (10 cm versus 4 cm for Robeson Channel) and thicker ice (183 cm versus 137 cm for Robeson Channel). Both spectra exhibit a rapid decrease in intensity with frequency, commencing in the frequency range 10–20 kHz, which is a result of the increase of the attenuation coefficient with frequency for $P$ waves in the sea ice. Below this frequency range the average slope of the intensity depends primarily on the attenuation coefficient in snow.

Assumptions made in calculating spectral responses were as follows: The snow layer is a hard, porous absorbent but transmits only $P$ waves. The ice layer is liquid. The snow grain impacts occur randomly and uniformly over the whole

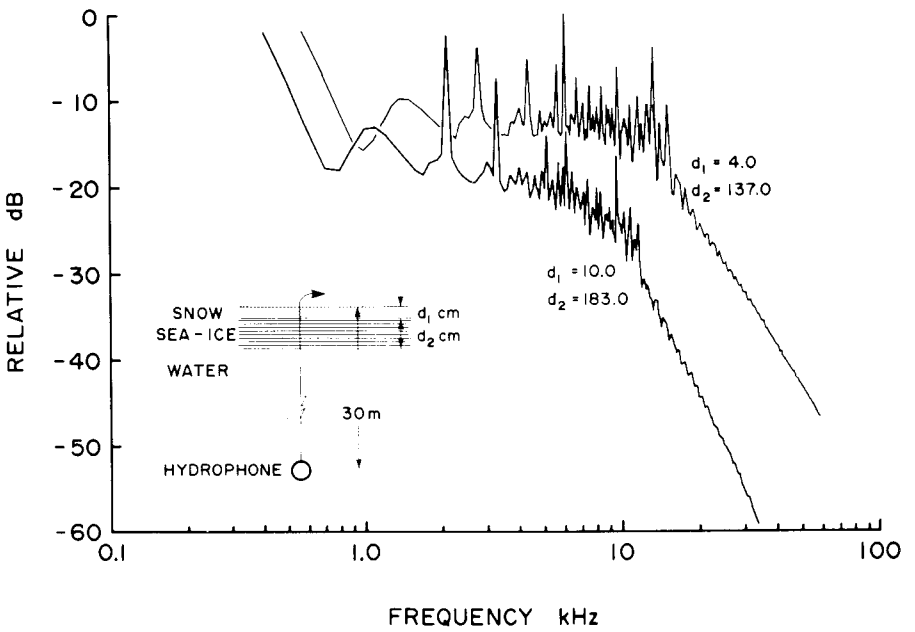


Fig. 11. Calculated underwater acoustic noise spectra for an omnidirectional hydrophone at a depth of 30 m. The upper curve is a prediction for the Robeson Channel site with a snow layer of 4-cm mean thickness and an ice layer of 137-cm thickness. The lower curve is a prediction for Lancaster Sound with a snow layer of 10-cm mean thickness and an ice layer of 183-cm thickness.

boundary separating the air and the snow layer and act as an infinite array of simple impulsive dipole sources with a pressure response proportional to the cosine of the angle of incidence to the plane of the layers. The plane upon which the impacts occur can be vertically translated an infinite distance above the actual impact plane without producing a change in the spectral density of the noise field detected beneath the ice. As a consequence of the latter translation, plane wave calculations of transmission loss are valid, provided contributions from all angles of radiation are summed and properly weighted.

Consequent to the above assumptions, plane wave transmission losses through the snow and ice layers were calculated at various angles of incidence by using *Berkhovskikh*'s [1960, p. 58] method, where attenuation coefficients were introduced by the use of complex wave numbers. For snow, assumed to be a hard, porous absorbent [*Ford et al.*, 1967], the complex wave number has the form $k_1 = (\omega/\alpha_0)\,[1 + i\epsilon/(\omega\rho_0)]^{1/2}$, where $\alpha_0$ is the speed of sound in air, $\rho_0$ is the density of air, $\omega$ is the circular frequency, $i = (-1)^{1/2}$, and $\epsilon$ is a coefficient of viscous friction. It can be shown that for $\omega > 10^3$, $\epsilon = (2\eta\omega\rho_0)^{1/2}/a_d$, where $\eta$ is the viscosity coefficient for air and $a_d$ is an effective dynamic pore radius between particles [*Morse*, 1952]. For $\eta = 181.2 \times 10^{-6}$ dyne sec cm$^{-2}$, $\rho_0 = 1.3 \times 10^{-4}$ g cm$^{-3}$, and $\alpha_0 = 3.44 \times 10^4$ cm sec$^{-1}$, substituting for $\epsilon$ in the expression for $k_1$ and finally assuming large values of $\omega$, we obtain $k_1 \approx (\omega/\alpha_0) + i7.67 \times 10^{-6}\,\omega^{1/2}/a_d$. Here the imaginary part of $k_1$, identical to $\gamma_1$, is the attenuation coefficient in snow for high frequencies. *Morse* [1952] shows that $a_d \approx 0.125a$, where $a$ is the grain diameter. Using $a = 0.075$ cm, the mean grain diameter measured in Robeson Channel, $\gamma_1 \approx 8.18 \times 10^{-4}\,\omega^{1/2}$ Np cm$^{-1}$ for high frequencies. This result for $\gamma_1$ checks surprisingly well with high-frequency attenuations measured in snow during April 1971 in Robeson Channel, where $\gamma_1 = 9.7 \times 10^{-4}\,\omega^{1/2}$ Np cm$^{-1}$ was obtained in similar snow. If the latter value of $\gamma_1$ is assumed for high frequencies, the complex wave number for the snow layer becomes

$$k_1 = (\omega/\alpha_0)(1 + 66.2i/\omega^{1/2})^{1/2} \quad \text{cm}^{-1}$$

Attenuation of longitudinal waves in sea ice has been measured by *Pounder and Langleben* [1968], where $\gamma_2 = 0.023\,(\log_{10}(\omega) - 4.93)$ Np cm$^{-1}$ for $\omega \geq 8.5 \times 10^4$ sec$^{-1}$ and $\gamma_2 \approx 0$ at lower frequencies. The resulting complex wave number used for sea ice was $k_2 = (\omega/\alpha_2) + 0.023i(\log_{10}(\omega) - 4.93)$ cm$^{-1}$ for $\omega \geq 8.5 \times 10^4$ sec$^{-1}$ and $k_2 = (\omega/\alpha_2)$ for $\omega < 8.5 \times 10^4$ sec$^{-1}$, where $\alpha_2$ is the speed of bulk longitudinal waves in the sea ice set equal to $3.5 \times 10^5$ cm sec$^{-1}$.

A similar complex wave number was used for the seawater beneath the ice, where the attenuation coefficient of *Schulkin and Marsh* [1962] was used.

## CONCLUSIONS

When the wind blowing over the snow on sea ice exceeds a threshold speed, it dislodges snow grains that saltate in a downwind direction. The impacts of the saltating grains cause noise that is transmitted to the water below the ice. The spectrum of the resulting noise detected by a hydrophone in the water appears to be the result of the impulse pressure response of the snow and ice layers and the water beneath to a set of random impulsive impacts caused by grain saltation. Once saltation commences, the shape of the spectrum tends to remain constant, but its intensity will rise at a rate approaching the cube of the wind speed. Theory indicates that the noise intensity is independent of the saltating grain size and depends solely on the total transport of grains. The crunching noise of footsteps on thin snow on sea ice appears to excite nondispersive *SV* waves, or Crary waves, which are trapped in the ice layer.

*Acknowledgments.* I am indebted to those who assisted in the data collection and analysis, particularly M. R. Black and F. D. Greensmith. Liberal support of the field operations was provided by

the Canadian Forces both at Canadian Forces Base Alert and in transportation to and from the North. All in-house support was provided by the Defence Research Board of Canada.

## REFERENCES

Bagnold, R. A., *The Physics of Blown Sand and Desert Dunes*, 265 pp., Methuen, London, 1941.

Brekhovskikh, L. M., *Waves in Layered Media*, 561 pp., Academic, New York, 1960.

Dyunin, A. K., Fundamentals of the mechanics of snow storms, in *Physics of Snow and Ice*, edited by H. Oura, p. 1065, Institute of Low Temperature Science, Hokkaido University, Sapporo, Japan, 1967.

Ewing, W. M., W. S. Jardetzky, and F. Press, Elastic waves in layered media, pp. 293–301, McGraw-Hill, New York, 1957.

Ford, R. D., B. V. Landau, and M. West, Reflection of plane oblique air waves from absorbents, *J. Acoust. Soc. Amer.*, *44*, 531, 1967.

Ganton, J. H., and A. R. Milne, Temperature and wind-dependent ambient noise under midwinter pack ice, *J. Acoust. Soc. Amer.*, *38*, 406, 1965.

Milne, A. R., Thermal tension cracking in sea ice: A source of underice noise, *J. Geophys. Res.*, *77*, 2177, 1972.

Milne, A. R., J. H. Ganton, and D. J. McMillin, Ambient noise under sea ice and further measurements of wind and temperature dependence, *J. Acoust. Soc. Amer.*, *41*, 525, 1967.

Morse, R. W., Acoustic propagation in granular media, *J. Acoust. Soc. Amer.*, *24*, 696, 1952.

Oura, H., T. Ishida, D. Kobayashi, S. Kobayashi, and T. Yamada, Studies on blowing snow, 2, in *Physics of Snow and Ice*, edited by H. Oura, p. 1099, Institute of Low Temperature Science, Hokkaido University, Sapporo, Japan, 1967.

Pounder, E. R., and M. P. Langleben, Acoustic attenuation in sea ice, *Publ. 79*, pp. 161–169, Int. Ass. Sci. Hydrol., 1968.

Schulkin, M., and H. W. Marsh, Sound absorption in seawater, *J. Acoust. Soc. Amer.*, *34*, 864, 1962.

(Received August 15, 1973;
revised October 16, 1973.)